Monthly Notices of the ROYAL ASTRONOMICAL SOCIETY

MNRAS **492,** 2709–2721 (2020) doi:10.1093/mnras/stz3616
Advance Access publication 2020 January 3

A study of the physical properties of SB2s with both the visual and spectroscopic orbits

Luca Piccotti [1,2★] José Ángel Docobo,[1,2,3] Roberta Carini,[4★] Vakhtang S. Tamazian,[1] Enzo Brocato [4,5] Manuel Andrade[1,2,6] and Pedro P. Campo[1,2★]

[1]*Observatorio Astronómico Ramón María Aller, Universidade de Santiago de Compostela (USC), Avenida das Ciencias s/n, Campus Vida, Santiago de Compostela, E-15782 Galiza, Spain*
[2]*Instituto de Matemáticas and Departamento de Matemática Aplicada, Facultade de Matemáticas, USC, Ría Lope Gímez de Marzoa, s/n, Campus Vida, Santiago de Compostela, E-15782 Galiza, Spain*
[3]*Real Academia de Ciencias de Zaragoza, Facultad de Ciencias, Universidad de Zaragoza, C/ Pedro Cerbuna 12, E-50009 Zaragoza, Spain*
[4]*INAF, Osservatorio Astronomico di Roma, Via di Frascati, 33, I-00078 Monteporzio Catone, Italy*
[5]*INAF, Osservatorio Astronomico d'Abruzzo, Via Mentore Maggini, s.n.c., Loc. Collurania, I-64100 Teramo, Italy*
[6]*Escola Politécnica Superior de Enxeñaría, USC, Benigno Ledo s/n, Campus Terra, Lugo, E-27002 Galiza, Spain*

Accepted 2019 December 20. Received 2019 December 20; in original form 2019 July 2

ABSTRACT

The study of a selected set of 69 double-lined spectroscopic binaries (SB2) with well-defined visual and spectroscopic orbits was carried out. The orbital parallax, the mass, the colour, and the luminosity of each component were derived from observational data for almost all of these systems. We have also obtained an independent estimation of the component masses by comparing the colour–magnitude diagram (CMD) to the stellar evolution tracks reported by Pietrinferni. Nearly all of the observational points on the CMD are located between two tracks of slightly different mass or which fall very close to the one corresponding to a unique mass value. The masses obtained from the stellar model are in good agreement with their empirical values determined by parallax techniques (orbital, *Gaia*, and dynamical). This means that our adopted model is rather reliable and can therefore be used to infer further information, such as the age of each component in the studied systems. Our results indicate a fair correspondence between the age of primaries and secondary stars within 3σ. Nevertheless, we caution that these age indications suffer of uncertainties due to both inhomogeneities/low precision of the adopted photometric data and possible systematics. Finally, it is statistically shown that along with the orbital and trigonometric parallaxes, the dynamical parallax can serve as a reliable tool for distance estimates.

Key words: binaries: spectroscopic – binaries: visual – stars: fundamental parameters.

1 INTRODUCTION

The knowledge of both the visual and the spectroscopic orbits in binary systems is very important for stellar astronomy since the combined analysis of astrometric and spectroscopic observations produces, without any additional assumptions, a complete 3D binary orbit, enabling precise distance, luminosity, and masses of the system components to be determined (McAlister 1976, 1977, 1978; Balega, Bonneau & Foy 1984; Barlow, Fekel & Scarfe 1993; Pourbaix 1998; Scarfe, Barlow & Fekel 2000; Torres 2004; Boden, Torres & Latham 2006; Docobo et al. 2014, 2018; Docobo, Campo & Horch 2017; Fekel, Henry & Tomkin 2017). In turn, the use of these fundamental parameters allow to make valuable comparisons with stellar evolutionary models (Claret & Gimenez 1992; Palla & Stahler 1999; Girardi et al. 2000; Siess, Dufour & Forestini 2000; VandenBerg, Bergbush & Dowler 2006; Claret 2007; Bressan et al. 2012; Baraffe et al. 2015).

The obtained masses and luminosities are especially important for testing models for stars at the lower part of the main sequence populated by low-mass stars, brown dwarfs, and other objects in the substellar mass regime, yet they are crucial to compare the theories that are being developed for their formation and evolution (Baraffe et al. 1998, 2015; Palla & Stahler 1999). Moreover, orbital parallaxes deduced from definitive 3D orbits serve as a solid test (Docobo et al. (2014, 2018) for the *Gaia* parallaxes (Gaia Collaboration 2016, 2018).

The possibilities for the direct determination of stellar masses and precise orbital parallaxes from their 3D orbits have been greatly enhanced over the past several decades due to the overlap

★ E-mail: l.piccotti@usc.es (LP); roberta.carini@oa-roma.inaf.it (RC); pedropablo.campo@usc.es (PPC)

of spectroscopic and visual binaries that are observable with both spectroscopy- and ground-based optical and near-infrared interferometry. At present, in some cases the derived component masses are already at the <1–2 per cent precision level sufficient to constrain modern main-sequence and post-main-sequence stellar models (Torres, Andersen & Gimenez 2010). In particular, Barry, Demory & Segransan (2012) reported the 0.4 per cent precision on the individual masses of the double-lined spectroscopic M-dwarf binary, Gliese 268, obtained from the high-precision interferometric and radial velocity observations.

A large number of astrometric orbits of the stars from the 9th Catalogue of Spectroscopic Binary orbits (hereinafter SB9, Pourbaix et al. 2004) has been presented by Jancart et al. (2005) using the *Hipparcos* Intermediate Astrometric Data (IAD). These authors noticed, however, that reported astrometric orbits cannot in general be derived from the IAD for double-lined spectroscopic systems and therefore no fully consistent stellar masses can be obtained for their components.

The goal of the present investigation is, on the one hand, to obtain the orbital parallaxes of those visual binaries with definitive or almost definitive orbit, grades 1 and 2 in the Sixth Catalog of orbits of Visual Binary Stars (hereinafter ORB6, Hartkopf, Mason & Worley 2001a), and which are also double-lined spectroscopic binaries (SB2) with orbit (including those in the SB9, Pourbaix et al. 2004). These parallaxes are data of great reliability and, therefore, constitute an excellent test to compare with those measured by the *Hipparcos* and *Gaia* spacecrafts. On the other hand, the values of the masses of each component can also be calculated with high precision separately for this selected set of binaries.

Taking into account all values of parallaxes and masses obtained, it can be derived from them absolute magnitudes, which, together with the spectral types, allow a study of the evolutionary tracks of each component of the systems studied.

In this article, we present the study of 69 binary stars: among these, 57 have also published *Gaia*'s parallax, out of which 42 systems belonging to the main sequence, nine with at least one component of luminosity class IV, and eight with at least one component of luminosity class III.

After Introduction, we present the calculation process in Section 2. The orbit list compilation procedure is described in Section 3. We also carried out, in Section 4, a statistical study of all parallaxes in order to compare the orbital parallaxes with other parallax values. Indeed, in this sample there are many stars with trigonometric parallaxes measured in the *Gaia* mission ($\pi''_{\rm Gaia}$) for which it is also possible to calculate orbital ($\pi''_{\rm Orb}$) and dynamical parallaxes ($\pi''_{\rm Dyn}$). This is a sample of 48 binary systems which, belonging to the main sequence or to the group of the subgiants stars, have visual orbits graded 1 or 2 in the ORB6 (Hartkopf, Mason & Worley 2001a) along with double-lined spectroscopic orbits (SB2) in the SB9 (Pourbaix et al. 2004). In Section 5, we provide a completely independent evaluation of the masses of primary and secondary stars of each binary system. Finally, in Section 6, we draw conclusions.

In the paper version, for both tables and graphs, we publish the data related to the first 10 systems; the remaining ones will be published online.

2 THE CALCULATION PROCESS

From the elements of both orbits, for each binary of the list, we have determined their orbital parallax, the corresponding individual masses, and other physical parameters, according to the following calculation sequence:

2.1 Calculation of the semimajor axis of the orbit in Astronomical Units

Starting from the data of the spectroscopic orbit, we have:

$$a \sin i = a_1 \sin i + a_2 \sin i, \tag{1}$$

in km, and:

$$a \sin i_{(\rm au)} = a \sin i_{\rm km} / 149\,597\,870.700, \tag{2}$$

in astronomical units (au), where a_1 and a_2 are the semimajor axis of the first and the second components, respectively, with respect to the centre of mass of the system, and $a = a_1 + a_2$.

From the value of $a \sin i$ expressed in au, it is possible to determine the value of the orbital semiaxis in astronomical units by means of:

$$a_{(\rm au)} = \frac{a \sin i_{(\rm au)}}{\sin i}, \tag{3}$$

where the sine of the inclination of the visual orbit appears in the denominator.

2.2 Determination of the orbital parallax and individual masses

In these conditions, taking into account that a' is the semimajor axis of the visual orbit expressed in seconds of arc, we deduce the orbital parallax according to:

$$\pi''_{\rm Orb} = \frac{a''}{a_{(\rm au)}}. \tag{4}$$

Starting from here, the masses of each component were obtained separately. In effect, the mass ratio (q) is known from the spectroscopic orbit:

$$q = \frac{\mathcal{M}_1}{\mathcal{M}_2} = \frac{a_2}{a_1} = \frac{a_2 \sin i}{a_1 \sin i}, \tag{5}$$

where $\mathcal{M}_1$ is the mass is the mass of the primary and $\mathcal{M}_2$ is the mass of the secondary.

Then, using *Kepler*'s Third Law:

$$\mathcal{M}_1 + \mathcal{M}_2 = \left(\frac{a''}{\pi''_{\rm Orb}}\right)^3 \left(\frac{1}{P^2}\right) = \frac{a^3}{P^2}, \tag{6}$$

with a in au and P in yr, we also have the sum of masses and, therefore, the mass of each component:

$$\begin{aligned} \mathcal{M}_2 &= \left(\frac{1}{1+q}\right)(M_1 + M_2), \\ \mathcal{M}_1 &= q\, M_2 \end{aligned} \tag{7}$$

in solar masses ($\mathcal{M}_\odot$).

2.3 Calculation of the masses taking into account other values of the parallaxes

After the determination of the mass of each component using the orbital parallax, we will compare the masses calculated with the parallaxes measured by *Gaia* or *Hipparcos* (van Leeuwen et al. 2007).

Likewise, we have deduced the dynamical parallaxes for the stars belonging to the main sequence, as well as for the subgiants. These values and the masses deduced from them give us an idea of the verification of the mass–luminosity diagram by them. In addition, it has recently been demostrated (Andrade et al. 2019) that using a non-linear mass–luminosity relationship (MLR) fit, dynamical parallaxes are a very useful indicator of distances.

For the calculation of the dynamical parallax, the spectral types of the two components included in the SB9 catalogue were taken into account. In the cases in which only the composite spectrum was available, it was unfolded using the Edwards Process (Edwards et al. 1976).

In order to apply this process, the value of the magnitude difference, Δm, between the components was taken from the speckle measurements collected in the Fourth Catalog of Interferometric Measurements of Binary Stars (INT4; Hartkopf, McAlister & Mason 2001b).

The apparent magnitudes of the two components were calculated from the combined (or total) magnitude in the visual band, m_t (taken from Set of Identifications, Measurements and Bibliography for Astronomical Data (SIMBAD)) and using the information of Δm provided by INT4. In these conditions, the individual magnitudes have been obtained by means of the expressions:

$$\begin{aligned} m_1 &= m_t + 2.5\log_{10}(1+10^{0.4\Delta m}),\\ m_2 &= m_1 + \Delta m. \end{aligned} \tag{8}$$

Interstellar extinction A_V was estimated with the Parenago formula (Parenago et al. 1940; Malkov et al. 2018), relating A_V with distance (r) and galactic latitude (b):

$$A_V = \frac{a_0\beta}{|\sin b|}\left[1-e^{-\frac{r|\sin b|}{\beta}}\right], \tag{9}$$

where β is the scale height and a_0 is the extinction to an object located in the galactic plane behind the absorbing layer. The values of 1.6 mag kpc^{-1} and 114 pc were accepted for a_0 and β, respectively, according to Sharov's study (Sharov et al. 1964). Using the interstellar extinction, the absolute magnitudes, in the visual band, are calculated using the formula:

$$M_V = m + 5 + 5\log_{10}(\pi''_{Orb}) - A_V, \tag{10}$$

where π''_{Orb} is the orbital parallax obtained by us according to the calculation process explained in paragraphs 1 and 2 of this section.

Once the absolute magnitudes in the visual of the two components, M_{V_1} and M_{V_2}, were known, we found the absolute magnitudes in the blue of the two components, M_{B_1} and M_{B_2}, directly from the colour index, $B-V$:

$$\begin{aligned} M_{B_1} &= (B_1 - V_1) + M_{V_1}\\ M_{B_2} &= (B_2 - V_2) + M_{V_2} \end{aligned} \tag{11}$$

We have also added the distances in parsecs for each binary system, once the parallaxes have been known:

$$d = \frac{1}{\pi''} \tag{12}$$

2.4 Calculation of the dynamical parallax and individual masses

We have also calculated the dynamical parallax for the stars belonging to the main sequence, as well as for the subgiants. These values and the masses deduced from them give us an idea of the verification of the mass–luminosity diagram.

The Baize–Romani algorithm (Baize & Romani, 1946) allows us to calculate the dynamical parallax, π''_{Dyn}, and the masses from the orbital elements, in particular the semimajor axis, a', and the period, P, the magnitudes, and the spectral types, by using an MLR.

Taking into account *Kepler*'s Third Law:

$$\mathcal{M}_1 + \mathcal{M}_2 = \left(\frac{a''}{\pi''_{Dyn}}\right)^3 \frac{1}{P^2}, \tag{13}$$

where $\mathcal{M}_j$, with $j = 1, 2$, represents the mass of the jth component, if we call $h^3 = (\mathcal{M}_1 + \mathcal{M}_2)\pi''^3_{Dyn}$, then:

$$\log(h) = \log(a'') - \frac{2}{3}\log(P). \tag{14}$$

If we consider an MLR of the type:

$$L \propto \mathcal{M}^k, \tag{15}$$

where L is the luminosity, $\mathcal{M}$ the mass, and k a coefficient, we can reformulate the relationship in terms of magnitudes, as follows:

$$M_{bol} = M_{bol,\odot} - \frac{5}{2}\,k\,\log(\mathcal{M}), \tag{16}$$

here M_{bol} is the bolometric magnitude.

Taking into account that $M_{bol} = M_V + BC$, where M_V is the visual magnitude and BC represents the bolometric correction, and the known relationship between the absolute (M) and apparent (m) magnitudes, $M = m + 5 + 5\log(\pi'')$, we can combine these formulae with equations (13) and (16) to obtain the dynamical parallax:

$$\log(\pi''_{Dyn}) = \log(h) + \frac{0.4}{3\,k-2}(m_t + C + D + 5\log(h)) \tag{17}$$

being m_t the combined magnitude of the system, and:

$$C = BC + 5 - M_{bol,\odot} \tag{18}$$

$$D = \frac{5}{2}\left(\log(1+10^{0.4\,\Delta m_B}) + k\log(1+10^{0.4\,\Delta m_B/k})\right) \tag{19}$$

In order to apply these equations it is necessary to know the magnitude difference between the components, Δm, and the bolometric corrections, BC_1 and BC_2, for which we need the spectral types. There are also two parameters dependent on the MLR, k, and $M_{bol,\odot}$, for which we have adopted the values proposed in Docobo & Andrade (2013).

Now, *Kepler*'s Third Law and the MLR yield the individual masses:

$$\log(\mathcal{M}_1 + \mathcal{M}_2) = 3\log(h) - 3\log(\pi''_{Dyn}) \tag{20}$$

$$k\,\log\left(\frac{\mathcal{M}_1}{\mathcal{M}_2}\right) = 0.4\Delta M \tag{21}$$

2.5 Physical parameters

Notes about the particular type of objects (variable stars and variability class, eclipsing, etc.) were taken from the SIMBAD astronomical data base. Also from the same data base, magnitudes in the different bands (U, B, V, R, I, G, J, H, L, u, g, r, i, z) were taken for each of the binary systems in the list.

The information on the metallicity and the effective temperature was extracted from Casagrande et al. (2011).

Throughout the calculation sequence of the single quantities, uncertainties were evaluated using the error propagation formulas.

3 THE ORBITS LIST COMPILATION

To compile the orbit list, we combined data from both ORB6 and SB9. Table 1 lists the orbital elements common to the two catalogues: hereafter, for each star, the first two upper rows

Table 1. ORB6 and SB9 common orbital elements. First 10 VB–SB2 stars in the list. The full table is available online. For all spectroscopic orbits, grades of old orbits are taken from SB8 (5-best, 1-worst), for new orbits they are not entered, pending a development of new automatic grading system.

	WDS HD	Discover designation	P (d)	T (MJD)	e	ω (deg)	Gr	Orbit authors
ORB6	00084 + 2905	MKT 11Aa,Ab	96.7015	58784.4840	0.5350	257.4000	2	Pourbaix (2000)
			± 0.0044	± 0.0950	± 0.0046	± 0.3100		
SB9	358		96.7080	58786.1120	0.5400	259.0000		Catanzaro & Leto (2004)
			± 0.0030	± 0.5000	± 0.0400	± 1.0000		
ORB6	00352−0336	HO 212AB	2516.6163	56935.2034	0.7730	283.8000	1	Mason & Hartkopf (2005)
			± 2.7808	–	–	–		
SB9	3196		2527.0000	56972.3000	0.7700	289.0000		Duquennoy & Mayor (1991)
			Fixed	± 3.9000	–	± 3.1000		
ORB6	00369 + 3343	MKT 1Aa,Ab	143.5300	58705.0279	0.5420	170.7000	1	Hummel et al. (1995)
			± 0.0600	± 0.4000	± 0.0060	± 0.7000		
SB9	3369		143.6065	58773.4645	0.5600	169.0000	5	Pearce (1936)
			–	–	–	–		
ORB6	00373−2446	BU 395	9138.7142	56999.2800	0.2180	318.1000	1	Hartkopf & Mason (2010)
			± 10.0980	–	–	–		
SB9	3443		9165.6400	51144.7600	0.2352	317.0450	5	Pourbaix (2000)
			± 10.5920	± 60.2212	0.0096	2.8000		
ORB6	00572 + 2325	MKT 2Aa,Ab	115.7200	58753.8869	0.0060	215.0000	1	Hummel et al. (1993)
			± 0.0100	± 1.0958	0.0020	4.0000		
SB9	5516		115.7330	58795.3490	0.0032	283.0000		Massarotti et al. (2008)
			± 0.0230	± 24.0000	± 0.0044	± 75.0000		
ORB6	01376−0924	KUI 7	10530.3409	57322.8955	0.7480	248.8000	2	Tokovinin (1993)
			± 91.3141	± 7.6704	± 0.0050	± 0.3000		
SB9	10009		10540.0000	58404.2000	0.7976	251.5979	5	Pourbaix (2000)
			± 281.2360	± 4.2509	± 0.0066	± 0.6700		
ORB6	01379−8259	TOK 426	638.6909	58716.0025	0.1912	151.2000	2	Tokovinin (2016)
			± 0.1717	± 1.0958	0.0018	0.3000		
SB9	10800		638.6662	58818.9020	0.1912	151.1600		Tokovinin (2016)
			± 0.0005	± 0.0026	± 0.0018	± 0.5800		
ORB6	01546 + 2049	MKT 3	106.9944	58821.8485	0.8801	204.9000	2	Pourbaix (2000)
			± 0.0007	± 0.1826	± 0.0008	± 0.3300		
SB9	11636		106.9940	58824.8140	0.8802	204.9302	5	Pourbaix (2000)
			± 0.0007	± 0.0064	± 0.0008	± 0.3300		
ORB6	02095 + 3459	MKT 4	31.3870	58823.3889	0.4400	298.1000	1	Hummel et al. (1995)
			± 0.0010	± 2.5568	± 0.0020	± 0.2000		
SB9	13161		31.3891	58808.9637	0.4330	298.1300	5	Pourbaix (2000)
			± 0.0002	± 0.0322	± 0.0041	± 0.6600		
ORB6	02171 + 3413	MKT 5Aa,Ab	10.0197	58819.7386	0.0110	171.0000	1	Pourbaix (2000)
			± 0.0002	± 0.8000	± 0.0055	± 29.0000		
SB9	13974		10.0195	58817.9660	0.0107	171.9060	3	Pourbaix (2000)
			± 0.0002	± 0.7793	± 0.0055	± 29.0000		

represent ORB6 catalogue orbital elements and the two lower lines represent SB9 catalogue orbital elements. Column 1 specifies the catalogue: ORB6 or SB9. The second column gives the Washington Double Stars (WDS) code (coord. 2000) of the binary and below, its HD (Henry Draper) catalogue number. The system identifier adopted in the WDS ('discoverer designation' as a visual binary) is given in the third column. Columns 4–7 contain, for each catalogue, the orbital elements in the first line and their formal uncertainties in the following one: the orbital period, P, in days, the epoch of periastron passage, T, in MJD, the eccentricity, e, and the argument of periastron, ω, in degrees. The orbit grades are given in the ORB6 system, where 1 and 2 grades mean definitive and good orbits, respectively. The SB9 catalogue contains 2694 orbits of 2386 systems (SB1 and SB2) and 55 spectroscopic triple systems (http://sb9.astro.ulb.ac.be/). It provides easy access in order to search for the object using catalogues identifiers (HD, HIP, and BD), coordinates, publication's bibcod, etc. It lists the parameters of components, magnitudes, the spectral type, the orbital elements with their standard uncertainties, the orbit grades, and radial velocity curve. Grades of old orbits are taken from The Eighth Catalog of the orbital elements of Spectroscopic Binary stars (SB8; Batten, Fletcher & MacCarthy, 1989, 5-best, 1-worst), for new orbits they are not entered, pending a development of new automatic grading system. The last column contains references to the authors of the visual and spectroscopic orbits.

Hereafter, we will illustrate the tables with the data processed, according to the procedure described in the Section 2. Starting from

the second table in this article each system is identified by the HD number in the first column.

The semimajor axes, expresse in au, are listed in Table 2, where we have combined the visual and spectroscopic orbits, as we explained before using the equations (1)–(3). In columns 2–4, respectively, the values of a sin *i*, in km, a sin *i*, in au, and *a*, in au, appear with their uncertainties.

In Table 3, we compared the parallaxes: both the orbital and the dynamical one, calculated by us, with those provided by *Hipparcos* space mission and/or *Gaia* when available. We have for 16 systems the orbital parallax that falls within 3σ of the dynamic parallax, for 35 that falls within 3σ of the parallax of *Hipparcos* and for 23 that falls within 3σ of the parallax of *Gaia*. But, on the other hand, we have 45 systems whose orbital parallax falls within 3σ of at least one of the three parallax values (dynamical, *Hipparcos,* and *Gaia*). This discrepancy is probably due to the oldness of several spectroscopic orbits because the common orbital elements do not coincide perfectly with those of the visual orbit (see Table 1), and it is therefore desirable to recalculate a number of spectroscopic orbits. The orbital, *Hipparcos*, *Gaia*, and the dynamical parallaxes are given in columns 2–5, respectively, with their corresponding uncertainties.

In Table 3, we indicated with a (g) the stars that have a greater discrepancy from *Gaia* parallax (within the 3σ's *Gaia*) and when the latter was not published we indicated with a (h) the stars that have a greater discrepancy from *Hipparcos* parallax (within the 3σ's *Hipparcos*).

In Table 4, we illustrate the 11 binary stars of our list with a greater discrepancy: the orbital, *Hipparcos*, *Gaia*, and the dynamical parallaxes are found in columns 2–5, respectively, with their uncertainties.

In Table 5, we compared the individual masses of the two components of each system using the four parallaxes when available. The masses of the primary, using the orbital, *Hipparcos*, *Gaia*, and the dynamical parallaxes, are presented in columns 2–5, respectively, with their uncertainties; the masses of the secondary, using the orbital, *Hipparcos*, *Gaia*, and the dynamical parallaxes, are found in columns 6–9, respectively, with their uncertainties.

Table 6 collects the magnitudes in the visual band, calculated as described in equations (8)–(10). The description by columns is: (1) Henry Draper (HD) catalogue number; (2) composite apparent magnitude in the visual band, taken from the SIMBAD data base; (3) apparent magnitude of the primary in the visual band; (4) apparent magnitude of the secondary in the visual band; and (5) magnitude difference between the two components. This value was obtained averaging the corresponding data from speckle measurements collected in INT4 catalogue and discarding the extreme values; (6) composite absolute magnitude in the visual band without interstellar extinction; (7) absolute magnitude of the primary in the visual band without interstellar extinction; (8) absolute magnitude of the secondary in the visual band without interstellar extinction; (9) galactic latitude, in deg; (10) interstellar extinction, in mag; (11) interstellar reddening $E(B-V)$; (12) composite absolute magnitude in the visual band with interstellar extinction; (13) primary absolute magnitude in the visual band with interstellar extinction; and (14) secondary absolute magnitude in the visual band with interstellar extinction.

In Table 7, we collected the spectral types, temperatures, colour indices, and bolometric corrections (Gray et al. 2005). The description by columns is: (1) HD catalogue number; (2) spectral type of the primary; (3) class of the luminosity of the primary; (4) spectral type of the secondary; (5) class of the luminosity of the secondary; (6) effective temperature of the primary; (7) effective temperature of the secondary; (8) colour index $(B-V)$ of the primary; (9) colour index $(B-V)$ of the secondary; (10) colour index $(V-R)$ of the primary; (11) colour index $(V-R)$ of the secondary; (12) bolometric correction of the primary; and (13) bolometric correction of the secondary.

4 PARALLAXES

There are a number of stars with trigonometric parallaxes measured in the *Gaia* mission ($\pi''_{\rm Gaia}$) for which it is also possible to calculate orbital ($\pi''_{\rm Orb}$) and dynamical parallaxes ($\pi''_{\rm Dyn}$). This is a subsample of 48 binary systems commented before. This subsample was considered to carry out a validation of the *Gaia* parallaxes by comparison with dynamical parallaxes as well as with those obtained directly from the orbital elements. Some descriptive statistical data are summarized in Table 8. Our methodology is based on that described in Docobo & Andrade (2015) to analyse the accuracy of *Hipparcos* observations of binary systems.

4.1 Outlier detection

Since we are dealing with the most accurate trigonometrical parallaxes and, in addition, the orbital and the dynamical parallaxes have been derived from orbits for which major changes in the elements are not likely, one should not expect a large number of outliers. Nevertheless, a preliminary inspection of the differences (residuals) between *Gaia* parallaxes with respect to both the dynamical and the orbital parallaxes was accomplished using box and whisker plots (see Fig. 1). As a result, indices of all the mild and the extreme outliers are listed in Table 9. We note that residuals involving orbital parallaxes, specially those in the Orb–Gaia data set, show many suspected outliers either mild as extreme. In contrast, there are no extreme outliers and only four mild outliers in the Dyn–Gaia data set.

A further analysis of these outliers using the modified Thompson's τ technique (Thompson et al. 1935) confirmed that there were two statistically significant extreme outliers at the 99 per cent confidence level in the Orb–Gaia data set (HD 13974 and HD 76943) and one in the Orb–Dyn data set (HD 13974), being the latter a mild outlier of the Dyn–Gaia data set as well.

As usual, extreme outliers were deleted from the original data sets. Indeed, as explained in Section 4.2, the orbital parallax of HD 13974 system turned out to be an influential point that would have drastic effects on the linear regression model if it were not discarded. On the other hand, since mild outliers have proved to be barely significant in the statistical analysis that we carried out in this paper, its deletion was not justified. Therefore, the Dyn–Gaia data set would be the only one free of outliers.

4.2 Validation of the *Gaia* parallaxes

Gaia parallaxes were validated using the sample described in Section 4 and considering the linear regression model

$$\pi_{\rm Y} = a + b \cdot \pi_{\rm X} + \epsilon, \tag{22}$$

where $\pi_{\rm X}$ ($\pi''_{\rm Orb}$ or $\pi''_{\rm Dyn}$) is the independent variable and $\pi_{\rm Y}$ ($\pi''_{\rm Gaia}$) is the dependent variable. On the other hand, a and b are the unknown intercept and slope of the linear model, respectively. Finally, ϵ represents the scatter with relation to the regression line.

Parameter estimation in equation (22) was accomplished using an ordinary least–squares (OLS) method considering the various cases

Table 2. Calculated quantities. First 10 VB–SB2 stars in the list. The full table is available online.

HD catalogue number	(a sin *i*) (km)	(a sin *i*) (au)	*a* (au)
358	$(1.02973 \pm 0.047170) \times 10^8$	0.68833 ± 0.03153	0.71466 ± 0.03275
3196	$(6.06161 \pm 0.16101) \times 10^8$	4.05194 ± 0.10763	5.33661 ± 0.15336
3369	2.69784×10^8	1.80340	1.85083 ± 0.00149
3443	$(1.47715 \pm 0.04500) \times 10^9$	9.87412 ± 0.30081	10.07285 ± 0.30963
5516	$(5.88990 \pm 0.02280) \times 10^7$	0.39372 ± 0.00152	0.77574 ± 0.00967
10009	$(1.79500 \pm 0.06537) \times 10^9$	11.99882 ± 0.43696	12.09960 ± 0.44066
10800	$(2.32885 \pm 0.00514) \times 10^8$	1.55674 ± 0.00344	2.10811 ± 0.01679
11636	$(7.03286 \pm 0.03441) \times 10^7$	0.47012 ± 0.00230	0.63764 ± 0.00633
13161	$(3.79218 \pm 0.05805) \times 10^7$	0.25349 ± 0.00388	0.33043 ± 0.00515
13974	$(3.08171 \pm 0.05962) \times 10^6$	0.02060 ± 0.00040	0.07046 ± 0.01454

Table 3. Parallaxes. First 10 VB–SB2 stars in the list. The full table is available on-line. In the table we indicated with a (g) the stars that have a greater discrepancy from *Gaia* parallax (within the 3σ's *Gaia*) and when the latter was not published we indicated with a (h) the stars that have a greater discrepancy from *Hipparcos* parallax (within the 3σ's *Hipparcos*).

HD catalogue number	Orbital parallax (mas)	*Hipparcos* parallax (mas)	*Gaia* parallax (mas)	Dynamical parallax (mas)
358	33.5825 ± 1.5495	33.6200 ± 0.3500	–	34.1300 ± 0.3120
3196	45.1597 ± 1.3518	47.0500 ± 0.6700	–	52.4400 ± 0.1135 (h)
3369	3.6146 ± 0.0272 (g)	5.4500 ± 0.3100	5.9390 ± 0.3628	6.4000 ± 0.0544
3443	67.0118 ± 2.1350	64.9300 ± 1.8500	–	64.9500 ± 0.0622
5516	13.3680 ± 0.1711	14.2000 ± 0.2600	13.7059 ± 0.4251	
10009	24.1330 ± 1.1514	26.1500 ± 0.8100 (g)	24.0481 ± 0.4489	23.1600 ± 0.0672
10800	37.1091 ± 0.3701	36.5200 ± 0.2800 (g)	37.4167 ± 0.1415	42.8400 ± 0.1673 (g)
11636	56.4582 ± 0.6140	55.6000 ± 0.5800	–	55.8800 ± 0.4576
13161	24.2717 ± 0.4074 (h)	25.7100 ± 0.3400	–	
13974	139.0897 ± 28.7704 (g)	92.4100 ± 0.8200 (g)	90.8450 ± 0.3665	94.5700 ± 14.3711 (g)

Table 4. The 11 binary stars of our list with a greater discrepancy taking into account the values of the orbital parallax that fall at the same time out of 3σ of the dynamic, *Hipparcos* and *Gaia* parallaxes.

HD catalogue number	Orbital parallax (mas)	*Hipparcos* parallax (mas)	*Gaia* parallax (mas)	Dynamical parallax (mas)
13974	139.0897 ± 28.7704	92.4100 ± 0.8200	90.8450 ± 0.3665	94.5700 ± 14.3711
27991	22.1330 ± 0.9151	21.2000 ± 0.9200	18.9472 ± 0.2819	21.9000 ± 0.1764
40932	21.6211 ± 0.1404	21.0500 ± 0.6800	16.6954 ± 1.4291	25.4700 ± 0.0010
76943	56.3592 ± 1.0827	62.2300 ± 0.6800	71.1893 ± 1.4693	62.1000 ± 0.0071
157948	22.8532 ± 0.4998	19.7600 ± 0.8200	20.6764 ± 0.1141	22.6400 ± 0.3656
163840	36.3524 ± 0.5226	35.4000 ± 0.6200	30.8036 ± 0.4494	35.8100 ± 0.2617
184467	56.0971 ± 0.8230	59.8400 ± 0.6400	54.8715 ± 0.2400	57.3900 ± 0.4043
189340	39.5570 ± 5.6436	40.7500 ± 1.3500	46.9328 ± 0.9290	42.3100 ± 0.1205
202908	19.1759 ± 0.3138	20.9800 ± 0.5800	19.4425 ± 0.0665	22.2200 ± 0.0157
204236	16.9280 ± 0.3103	17.4800 ± 1.0200	15.3603 ± 0.2991	17.4300 ± 0.0064
209790	39.6797 ± 2.5088	38.1000 ± 2.8100	32.1697 ± 0.6211	29.6500 ± 0.7623

Table 5. Individual masses of the two components. First 10 VB–SB2 stars in the list. The full table is available online.

HD catalogue number	$\mathcal{M}_1$ ($\mathcal{M}_\odot$) Orb.	$\mathcal{M}_1$ ($\mathcal{M}_\odot$) Hip.	$\mathcal{M}_1$ ($\mathcal{M}_\odot$) *Gaia*	$\mathcal{M}_1$ ($\mathcal{M}_\odot$) Dyn.	$\mathcal{M}_2$ ($\mathcal{M}_\odot$) Orb.	$\mathcal{M}_2$ ($\mathcal{M}_\odot$) Hip.	$\mathcal{M}_2$ ($\mathcal{M}_\odot$) **Gaia**	$\mathcal{M}_2$ ($\mathcal{M}_\odot$) **Dyn.**
358	3.453 ± 0.661	3.441 ± 0.468	–	3.185 ± 0.437	1.755 ± 0.294	1.749 ± 0.174	–	1.619 ± 0.163
3196	1.925 ± 0.242	1.702 ± 0.167	–	1.175 ± 0.111	1.276 ± 0.141	1.129 ± 0.088	–	0.779 ± 0.057
3369	29.232 ± 0.930	8.528 ± 1.468	6.590 ± 1.217	4.835 ± 0.169	11.827 ± 0.376	3.450 ± 0.594	2.666 ± 0.492	1.956 ± 0.068
3443	0.938 ± 0.127	1.031 ± 0.133	–	1.005 ± 0.102	0.695 ± 0.082	0.764 ± 0.084	–	0.744 ± 0.058
5516	2.391 ± 0.098	1.995 ± 0.113	2.219 ± 0.209		2.259 ± 0.091	1.885 ± 0.106	2.096 ± 0.197	
10009	1.163 ± 0.230	0.914 ± 0.151	1.175 ± 0.174	1.334 ± 0.236	0.968 ± 0.179	0.761 ± 0.114	0.979 ± 0.127	1.111 ± 0.180
10800	2.032 ± 0.072	2.132 ± 0.064	1.982 ± 0.044	1.135 ± 0.033	1.032 ± 0.036	1.083 ± 0.032	1.007 ± 0.022	0.577 ± 0.016
11636	1.999 ± 0.079	2.093 ± 0.080	–	2.067 ± 0.057	1.023 ± 0.038	1.071 ± 0.039	–	1.058 ± 0.026
13161	3.514 ± 0.274	2.957 ± 0.211	–		1.372 ± 0.092	1.154 ± 0.068	–	
13974	0.246 ± 0.154	0.839 ± 0.060	0.884 ± 0.059	1.511 ± 0.123	0.219 ± 0.136	0.745 ± 0.045	0.785 ± 0.044	1.341 ± 0.097

Table 6. *V* magnitudes. All 69 VB–SB2 stars in the list. (1) HD catalogue number; (2) composite apparent magnitude in the visual band (*V*), taken from the SIMBAD data base; (3) apparent magnitude of the primary in the *V* band; (4) apparent magnitude of the secondary in the *V* band; and (5) magnitude difference between the two components. This value was obtained averaging the corresponding data from speckle measurements collected in INT4 catalogue and discarding the extreme values; (6) composite absolute magnitude in the *V* band without interstellar extinction; (7) absolute magnitude of the primary in the *V* band without interstellar extinction; (8) absolute magnitude of the secondary in the *V* band without interstellar extinction; (9) galactic latitude in deg; (10) interstellar extinction in mag; (11) interstellar reddening $E(B-V)$; (12) composite absolute magnitude in the *V* band with interstellar extinction; (13) primary absolute magnitude in the *V* band with interstellar extinction; and (14) secondary absolute magnitude in the *V* band with interstellar extinction.

(1)	(2)	(3)	(4)	(5)	(6)	(7)	(8)	(9)	(10)	(11)	(12)	(13)	(14)
358	2.060	2.221	4.211	1.990	− 0.309	− 0.148	1.842	−32.8433444	0.044423054	0.013882204	− 0.354	− 0.193	1.797
3196	5.201	5.488	6.788	1.300	3.475	3.761	5.061	−66.1487095	0.032461046	0.010144077	3.442	3.729	5.029
3369	4.360	4.383	8.538	4.155	− 2.850	− 2.826	1.329	−29.0545267	0.260010015	0.081253130	− 3.110	− 3.086	1.069
3443	5.570	6.168	6.504	0.336	4.701	5.298	5.634	−86.0493890	0.022383079	0.006994712	4.678	5.276	5.612
5516	4.420	4.936	5.476	0.540	0.050	0.566	1.106	−39.4349158	0.097877824	0.030586820	− 0.048	0.468	1.008
10009	6.240	6.563	7.712	1.149	3.153	3.477	4.626	−69.1892446	0.056210216	0.017565693	3.097	3.420	4.569
10800	5.870	6.313	7.056	0.743	3.717	4.161	4.904	−33.9988921	0.040388044	0.012621264	3.677	4.120	4.863
11636	2.650	2.712	5.789	3.077	1.409	1.471	4.548	−39.6817055	0.026979172	0.008430991	1.382	1.444	4.521
13161	3.000	4.191	3.441	− 0.750	− 0.075	1.117	0.367	−25.1984245	0.061099285	0.019093527	− 0.136	1.055	0.305
13974	4.870	4.886	9.446	4.560	5.586	5.603	10.163	−25.3829732	0.011349263	0.003546645	5.575	5.591	10.151

Note: Columns are numbered according to Section 3.

Table 7. Spectral types, temperatures, colour indices, and bolometric corrections. First 10 VB–SB2 stars in the list. The full table is available online. (1) HD catalogue number; (2) spectral type of the primary; (3) class of the luminosity of the primary; (4) spectral type of the secondary; (5) class of the luminosity of the secondary; (6) effective temperature of the primary; (7) effective temperature of the secondary; (8) colour index $(B-V)$ of the primary; (9) colour index $(B-V)$ of the secondary; (10) colour index $(V-R)$ of the primary; (11) colour index $(V-R)$ of the secondary; (12) bolometric correction of the primary; and (13) bolometric correction of the secondary.

(1)	(2)	(3)	(4)	(5)	(6)	(7)	(8)	(9)	(10)	(11)	(12)	(13)
358	B8	V	A7	V	11950.00	7935.00	− 0.06	0.22	− 0.02	0.19	− 0.60	0.02
3196	A4	V	F6	V	8532.33	6405.33	0.46	0.65	0.13	0.42	0.01	0.01
3369	B5	V	A9	V	14720.00	7430.33	− 0.24	− 0.24	− 0.06	0.26	− 1.08	0.03
3443	G8	V	K4	V	5486.00	4798.00	0.73	0.77	0.58	0.90	− 0.16	− 0.38
5516	G8	III	G8	III	5486.00	5486.00	0.93	0.93	0.70	0.70	− 0.33	− 0.33
10009	F9	V	G6	V	6051.50	5600.00	0.42	0.61	0.49	0.55	− 0.03	− 0.13
10800	A3	V	G2	V	8758.67	5811.00	0.58	0.67	0.11	0.53	0.01	− 0.08
11636	A3	V	G2	V	8758.67	5811.00	0.10	0.64	0.11	0.53	0.01	− 0.08
13161	A3	III	A8	III	8758.67	7682.67	0.07	0.21	0.11	0.23	0.01	0.03
13974	M3	V	M4	V	4025.00	3974.00	0.56	1.41	1.60	1.70	− 1.17	− 1.34

Note: Columns are numbered according to Section 3.

Table 8. Residuals in parallax differences: descriptive statistical data for the 56 binary systems.

	$\pi_{Orb} - \pi_{Gaia}$ (mas)	$\pi_{Orb} - \pi_{Dyn}$ (mas)	$\pi_{Dyn} - \pi_{Gaia}$ (mas)
Max.	14.83	5.77	10.43
Min.	− 48.24	− 44.52	− 8.78
Median	− 0.17	− 0.22	− 0.17
	{− 0.64, + 0.27}	{− 0.54, + 0.26}	{− 0.58, + 0.35}
MedianCI_{95} percent			
Mean	− 0.72	− 0.78	− 0.06
MeanCI_{95} percent	{− 2.70, + 1.25}	{− 2.51, + 0.95}	{− 0.81, + 0.93}
Trimean	− 0.44	− 0.43	− 0.05
Rmse	7.35	6.45	3.22
Correlation	0.9458	0.9641	0.9840

according to Table 9. The *a* and *b* parameters, their uncertainties, and the 95 per cent confidence intervals for each parameter together with the coefficient of determination (R^2) are summarized in Table 10. Thus, if these methods led to the same results, the dependence of π''_{Gaia} on both π''_{Orb} and π''_{Dyn} would be linear with zero intercept ($a = 0$) and unit slope ($b = 1$) considering the corresponding confidence intervals. This was automatically verified in the case of the Dyn–Gaia fit whereas, in the case of the Orb–Gaia, we had to previously discard the two extreme outliers. However, even doing that, the first fit was slightly better than the second.

Scatter plots with the OLS fits and the 95 per cent confidence intervals for both comparisons are shown in Fig. 2. The two

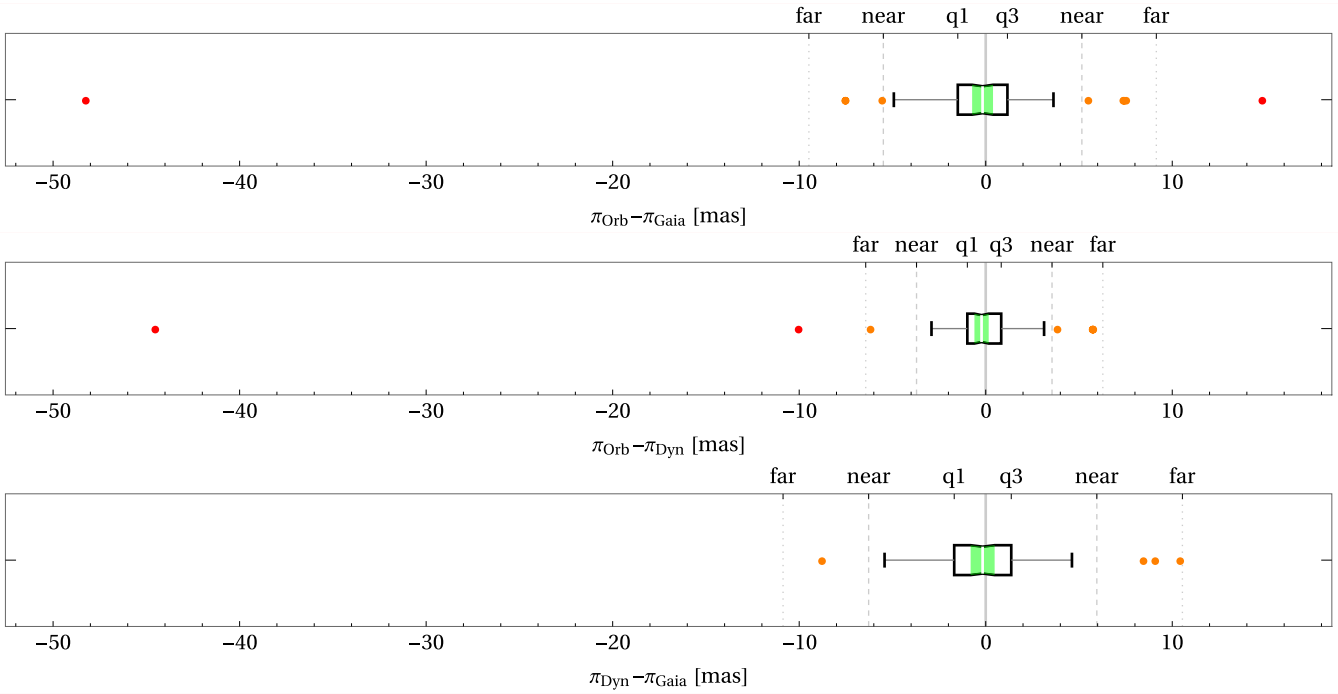

Figure 1. Boxplots of the differences between *Gaia* and dynamical parallaxes with respect to orbital ones (top and middle panels, respectively) along with differences between *Gaia* parallax with respect to dynamical ones (bottom panel). A thick white vertical bar indicates the median, whereas its confidence interval is shown in green. The vertical boundaries (or hinges) indicate the interquartile range (IQR). Thick line extensions (or whiskers) were, as usual, set at 1.5 × IQR above and below the 25 per cent (q1) and 75 per cent (q3) quartiles. Suspected mild outliers are shown as filled orange discs and extreme outliers as red discs.

Table 9. Positions of mild (indicated with round brackets) and extreme outliers detected in the residuals using box and whisker plots are listed in row 2, whereas those obtained using the modified Thompson's τ technique at the 99 per cent confidence level are listed in row 3. Finally, positions of the confirmed outliers (those extreme outliers common to the two analyses) are listed in the last row. Mild outliers are not taken into account in the statistical analysis (see the text).

Outliers $\pi_X-\pi_Y$	Orb–Gaia	Orb–Dyn	Dyn–Gaia
Box and whisker plot			
– Mild	(7), (10), (33), (35), (37), (43), (51)	(4), (7), (17), (19), (21)	(10), (17), (19), (21)
– Extrene	5, 21	5, 51	—
Thompson's τ	5, 17, 21	5, 17	5, 17, 21
Confirmed	5, 21	5	—

Table 10. Parameters for the OLS fits of the parallaxes ($\pi_Y = a + b \cdot \pi_X + \epsilon$) with the full data are listed in row 2 and those without outliers in row 3.

Fits	Orb–Gaia	Orb–Dyn	Dyn–Gaia
a (full data)	5.44 ± 1.37	5.33 ± 1.10	$+0.04 \pm 0.85$
CI[95 per cent]	$\{+2.68, +8.19\}$	$\{+3.11, +7.54\}$	$\{-1.66, +1.73\}$
b (full data)	0.80 ± 0.04	0.80 ± 0.03	1.00 ± 0.02
CI[95 per cent]	$\{+0.72, +0.87\}$	$\{+0.74, +0.86\}$	$\{+0.95, +1.05\}$
R^2	0.8946	0.9295	0.9682
a (w/o outliers)	0.76 ± 0.83	0.77 ± 0.70	
CI[95 per cent]	$\{-0.91, +2.43\}$	$\{-0.64, +2.17\}$	
b (w/o outliers)	0.97 ± 0.03	0.97 ± 0.02	[the same as above]
CI[95 per cent]	$\{+0.91, +1.02\}$	$\{+0.93, +1.02\}$	
R^2	0.9630	0.9743	

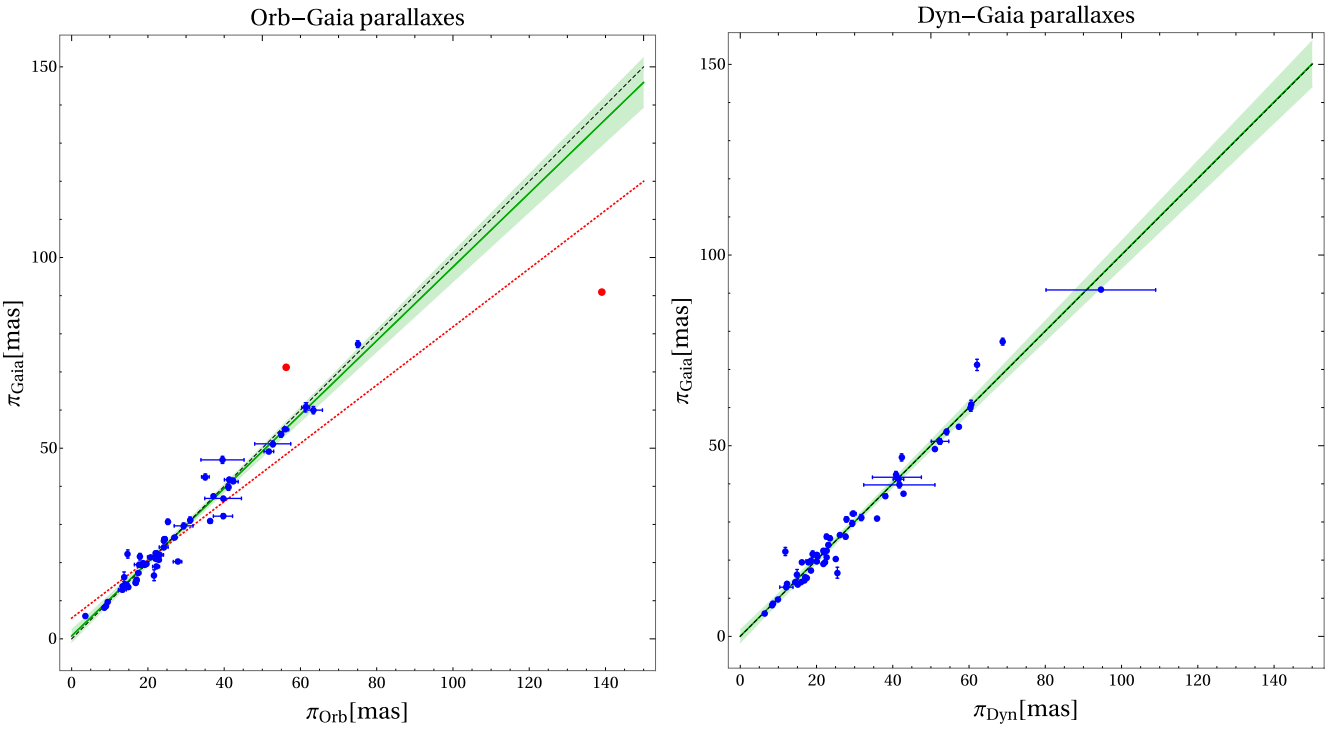

Figure 2. Scatter plot of Gaia versus orbital parallaxes (left) and dynamical parallaxes (right) for the 47 stars with visual orbits graded 1 or 2 in the ORB6 as well as with double-lined spectroscopic orbits (blue circles). Heteroscedastic measurement uncertainties in both variables are shown. A black dashed line indicates the perfect fit $\pi_Y = \pi_X$. The OLS fits of the observations (without outliers in the ORB–Gaia case) are indicated with a green solid line, whereas the 95 per cent confidence intervals are shown in light green. In addition, two extreme outliers are shown as red circles in the ORB–Gaia panel, whereas the OLS fit including them is indicated by the red dotted line.

extreme outliers in the Orb–Gaia data set are shown as red dots in the left-hand panel whereas the red line in this panel indicates the OLS fit including both outliers. We can easily see that the outlier placed on the right is an outlier in the independent variable, that is, a leverage point that has an extraordinary effect on the estimate of the regression coefficients. Actually, the R^2 value would decrease substantially from 0.9630 to 0.8946 if both outliers were not discarded.

On the other hand, *Gaia* parallaxes show a remarkable good fit to those obtained from the method of the dynamical parallaxes. As a matter of fact, its linear regression line ($\pi_{Gaia} = +0.04[\pm 0.85] + 1.00[\pm 0.02]\,\pi_{Dyn}$) matches almost exactly the perfect fit indicated by the diagonal black dashed line.

5 MASS EVALUATION FROM STELLAR EVOLUTION MODEL

In this section, we provide a completely independent evaluation of the masses of primary and secondary stars of each binary system. Taking advantage of the M_V and M_B absolute magnitudes available in the literature (taken from SIMBAD and from Gray et al. 2005) for the primary and secondary components, we derived two colour–magnitude diagrams (CMD), one including only primary components and the other representing the secondary ones (Fig. 3).

The basic idea is to compare the absolute magnitudes and colours obtained from observed binaries to the same quantities derived from a set of stellar evolution models. We use the evolutionary tracks by Pietrinferni and collaborators (http://basti.oa-teramo.inaf.it/) that were computed assuming a solar metallicity (Z=0.0198, $Y = 0.2734$, Pietrinferni et al. 2004). This choice is supported by the fact that the binary systems of our sample are all located in the proximity of the Sun. The evolution models used are calculated by adopting the Mixing Length treatment, while gravitational settling, radiative acceleration, convective overshooting, and rotational mixing are not considered. The mass-loss rate is in accord with Reimers (1975) law and the mass loss efficiency parameter, η, has been fixed at $\eta = 0.4$. The complete description of the theoretical models can be found in Pietrinferni et al. (2004). This set of evolutionary tracks provides a large number of models computed with very small differences in term of masses (the range of mass is between 0.5 and 10 $\mathcal{M}_\odot$). For this reason, nearly all the observational points in the CMD are contained between two tracks of slightly different masses or fall quite near to one track. It is then quite straightforward to identify the two tracks which contain the observational point. Each data point is then associated to the mass value of the nearest tracks. The uncertainty is given by the difference between the masses of the two closest tracks. Typically, our evaluation of the mass has an uncertainty on the order of 0.1 $\mathcal{M}_\odot$. Nevertheless, for the higher masses, the uncertainty increases to 0.25. This procedure is performed for the sample of primary stars and repeated for the secondary ones. The masses evaluated with the stellar evolution method are fully independent from the values of the masses obtained by dynamical and orbital arguments using *Hipparcos* and/or *Gaia* evaluations.

In Fig. 4, we plot the values obtained with the stellar evolution methods versus the orbital evaluations for primary and secondary components, respectively. Similarly, our *theoretical* mass values are compared to masses derived by dynamical quantities (Fig. 5) and *Gaia* measurements (Fig. 6). It appears quite clear that our *theoretical* masses are in good agreement with the masses evaluated by other independent methods, in particular with the dynamical

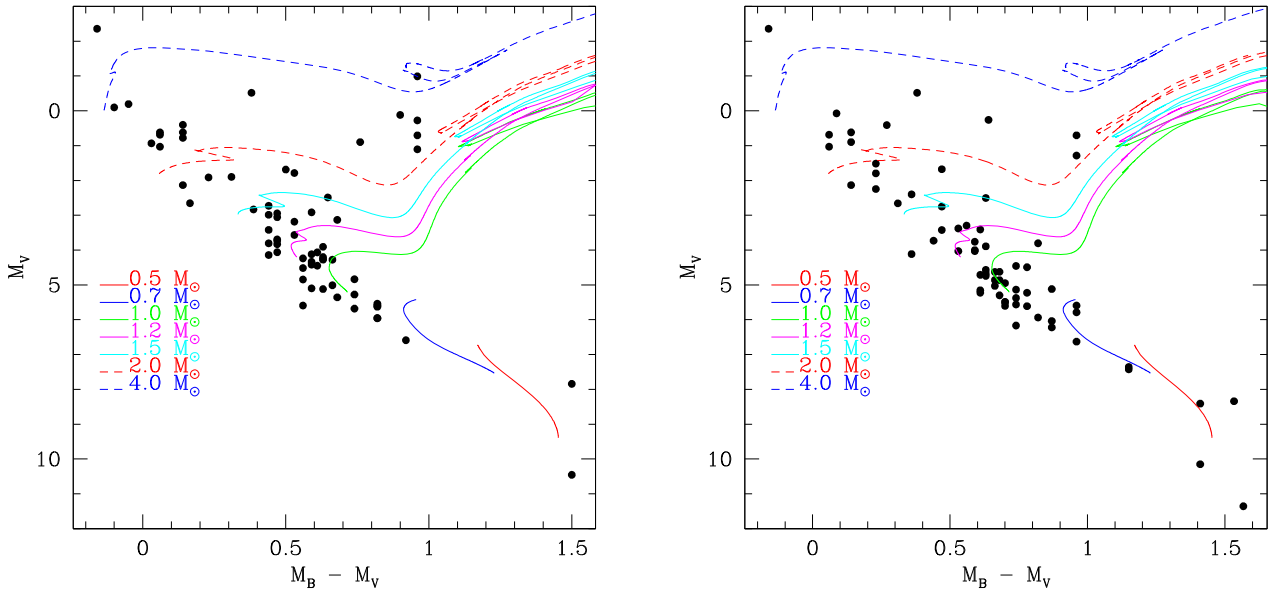

Figure 3. CMDs in *B* and *V* bands of the primary and secondary stars of the binary systems. The stellar evolutionary tracks used to derive the masses and ages (see the text) are overplotted, only a handful of them are shown for graphical clearness.

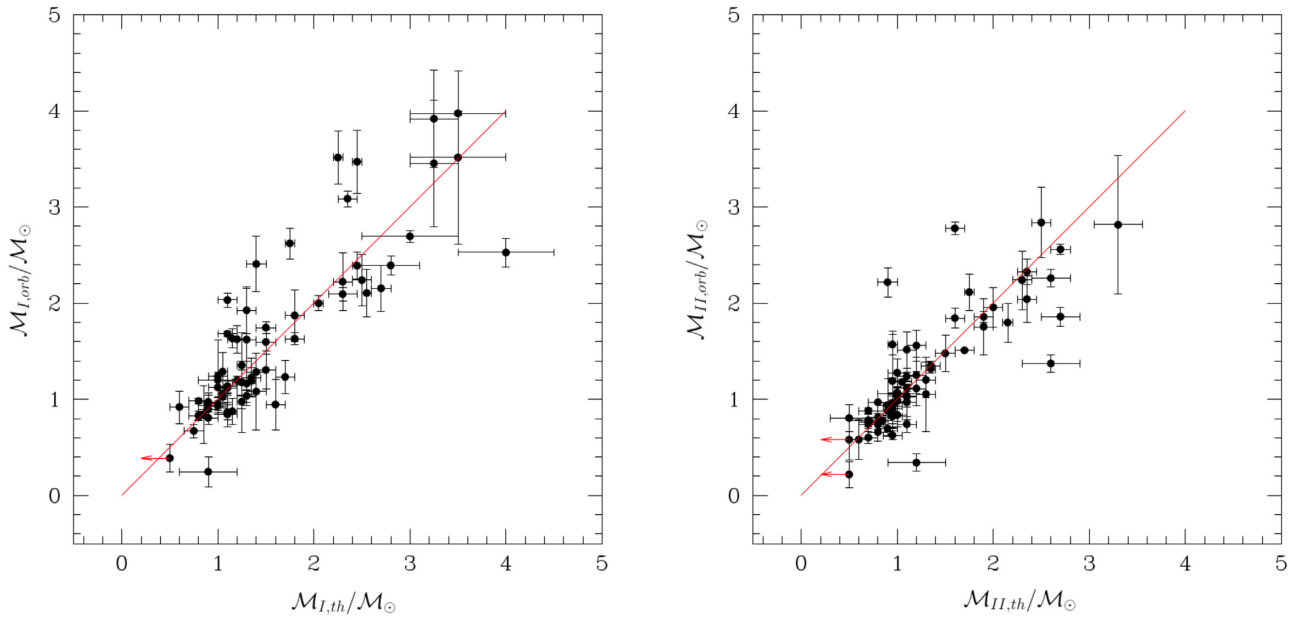

Figure 4. The mass of the primary (left) and secondary (right) stars obtained using our method of comparing evolutionary models to observed CMD is plotted against the masses derived using *Kepler*'s Third Law with orbital parallaxes. The red arrows represent the upper limit values. The line represents the full agreement between the two methods.

one. This is an interesting result because these values of masses can support the reliability of the stellar evolutionary models.

Once the evolutionary track is chosen to be representative of a given primary (or secondary) star from the CMD, it is straightforward to obtain the estimation of the age, the luminosity, and the effective temperature from the same theoretical model. The results for the primaries are represented in Table 11, and Table 12 provides the results for the secondary. The format of both tables is the same. Column 2 lists the mass in $\mathcal{M}_\odot$; in column 3, the logarithm of luminosity in $L_\odot$ is shown; in column 4, the logarithm of effective temperature appears, and finally, in column 5, the logarithm of age is given.

The independent results obtained concerning the ages of the primary and secondary stars allow us to provide indications about the contemporaneous formation of the two components of the binary systems. This is shown in Fig. 7 where the age of the primary stars is plotted against the secondary ones. Of course, we caution the reader about the systematic and intrinsic uncertainties which do not allow a solid conclusion. At first look at Fig. 7 shows some points are located above the red line (one to one correlation). We

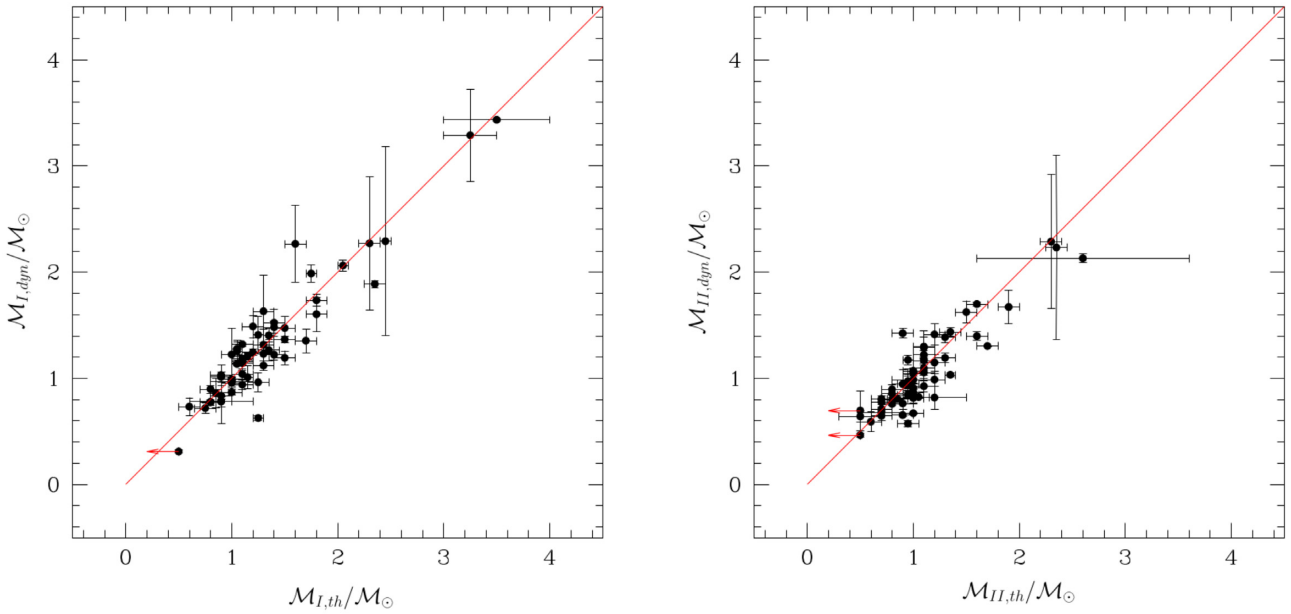

Figure 5. As in the Fig. 4, but for masses derived using *Kepler*'s Third Law with dynamical parallaxes.

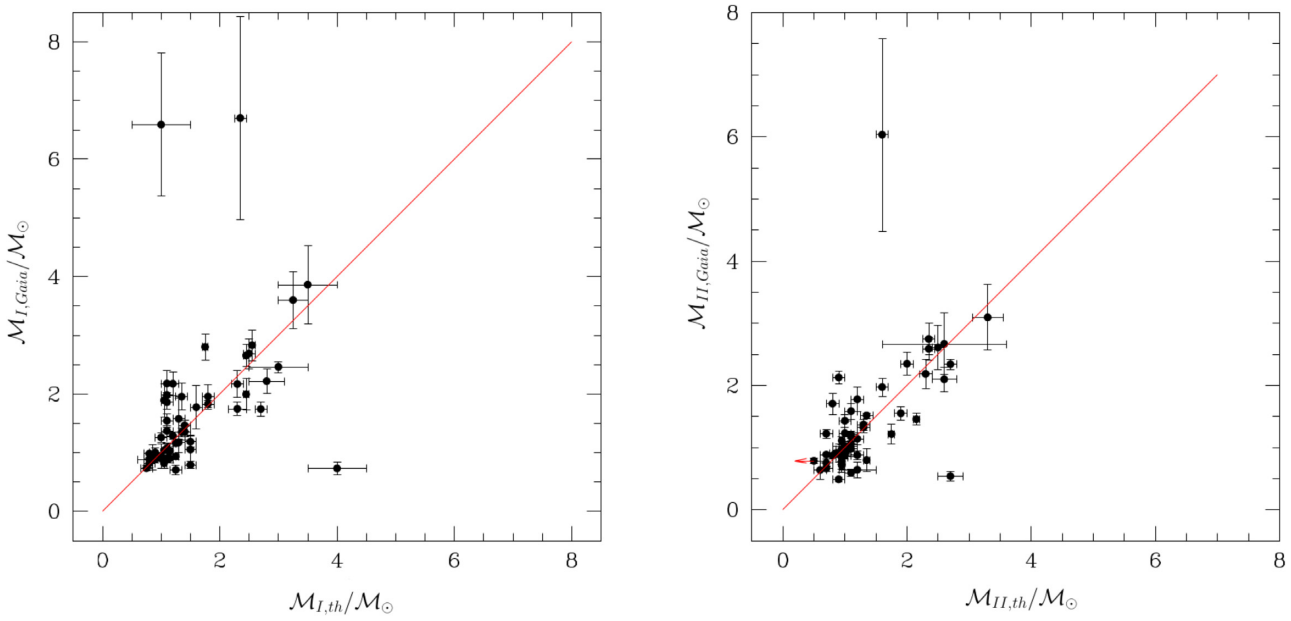

Figure 6. As in the Fig. 4, but for masses derived using *Kepler*'s Third Law with *Gaia* parallaxes.

caution to interpret this circumstance as a difference in age between primary and secondary stars in the studied binary systems. In fact, a possible explanation for this systematics is that the uncertainties in determining the ages are largely due to the assumed evolutionary tracks. As well known, the velocity of a stars in covering their evolutionary paths in the CMD is related to their masses, the more massive stars are much faster than the less massive, for this reason the faint stars (typically our secondary stars) are expected to suffer of systematically larger uncertainties in our age evaluation than the bright (typically our primaries) ones. In particular, even assuming the same error box in M_V and $(B-V)_0$ for primary and secondary stars, this affects in a different way the derived ages of the two components, i.e. larger uncertainties affect the fainter, less massive stars (typically our secondary stars) and this turn out to provide slightly older ages for those stars. A quantitative analysis suggests the ages of primaries are fairly well correlated to the ages of the secondary components, the slope of the best obtained using stars within 3σ is 0.95 ± 0.05 best fit. Obviously, larger sample of binaries and more precise measurements are needed to obtain more accurate results concerning the age determination.

6 CONCLUSIONS

1. An exhaustive study of 69 SB2s was carried out with both the visual and spectroscopic orbits well defined. By combining data from these orbits, we calculated the corresponding orbital parallaxes

Table 11. Estimation of masses and other physical quantities for the primaries. First 10 VB–SB2 stars in the list. The full table is available online.

HD catalogue number	($\mathcal{M}/\mathcal{M}_{\odot}$)	log L/$L_{\odot}$	log $T_{\rm eff}$	log (age)
358	3.25 ± 0.25	2.20 ± 0.10	4.02 ± 0.10	8.30 ± 0.20
3196	1.30 ± 0.10	0.42 ± 0.20	3.81 ± 0.05	8.20 ± 1.00
3369	10.00 ± 0.50	3.98 ± 0.10	4.33 ± 0.10	7.20 ± 0.10
3443	0.90 ± 0.10	−0.17 ± 0.10	3.74 ± 0.05	9.96 ± 0.15
5516	2.80 ± 0.30	1.80 ± 0.05	3.80 ± 0.10	8.80 ± 0.15
10009	1.30 ± 0.10	0.53 ± 0.10	3.81 ± 0.05	9.36 ± 0.30
10800	1.10 ± 0.10	0.26 ± 0.01	3.78 ± 0.02	9.70 ± 1.00
11636	2.05 ± 0.05	1.32 ± 0.10	3.93 ± 0.05	8.65 ± 0.20
13161	2.25 ± 0.05	1.50 ± 0.05	3.95 ± 0.05	8.65 ± 0.10
13974	0.90 ± 0.30	−0.28 ± 0.70	3.73 ± 0.10	9.63 ± 0.10

Table 12. Estimation of masses and other physical quantities for the secondaries. First 10 VB–SB2 stars in the list. The full table is available online.

HD catalogue number	($\mathcal{M}/\mathcal{M}_{\odot}$)	log L/$L_{\odot}$	log $T_{\rm eff}$	log (age)
358	1.90 ± 0.10	1.17 ± 0.10	3.90 ± 0.05	8.65 ± 0.15
3196	1.00 ± 0.10	−0.08 ± 0.50	3.76 ± 0.05	9.40 ± 0.50
3369	2.60 ± 1.00	1.66 ± 0.05	4.04 ± 0.15	7.20 ± 0.70
3443	0.90 ± 0.10	−0.29 ± 0.10	3.73 ± 0.05	9.60 ± 0.30
5516	2.60 ± 0.20	1.58 ± 0.10	3.71 ± 0.05	8.66 ± 0.15
10009	1.10 ± 0.10	0.09 ± 0.15	3.78 ± 0.05	9.00 ± 0.25
10800	1.00 ± 0.10	−0.01 ± 0.10	3.76 ± 0.05	9.68 ± 0.10
11636	1.10 ± 0.10	0.11 ± 0.05	3.78 ± 0.05	9.17 ± 0.70
13161	2.60 ± 0.30	1.78 ± 0.10	3.94 ± 0.10	8.60 ± 0.20
13974	< 0.50			

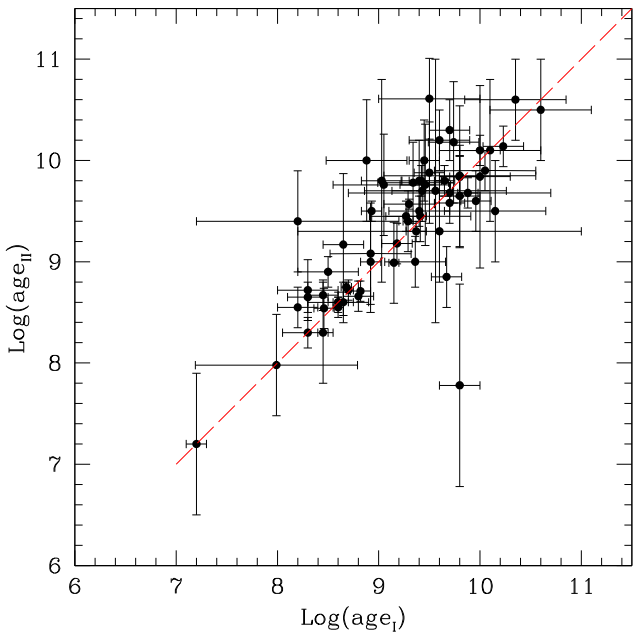

Figure 7. The age of primary stars versus the secondary ones is plotted. Both ages are derived with our theoretical method. The error bars refers to 1σ uncertainties, which do not account for possible systematics.

as well as the individual masses of the components. Moreover, the colour and the luminosity of each component were derived from observational data. The same parameters obtained with the use of the dynamical and *Gaia* parallaxes are generally in good agreement with derived values, except for those systems whose spectroscopic orbits were calculated many years ago. It would be desirable to recalculate these orbits.

2. We also conducted a statistical analysis by comparing the orbital parallax with the dynamical, *Gaia*, and *Hipparcos* parallaxes. Regarding dynamical parallaxes, our sample seems to be free of apparent outliers, at least of extreme outliers that could affect the analysis. Among other goals, this work has served to point out the necessity to obtain new precise measurements of radial velocities that permit, in various cases, the determination of spectroscopic orbits that are at least of a quality similar to the selected visual orbits. In this manner, the calculated orbital parallaxes would show their robustness and would be very close to the true parallaxes. On the other hand, the excellent fit between the *Gaia* and the dynamical parallaxes are notable in spite of the fact that the first are sometimes corrupted by the orbital motion. It is usually considered that the dynamical parallaxes contribute secondary information and that they are only useful when data concerning other parallaxes do not exit. However, recent research has indicated that, adopting a non-linear MLR and using an algorithm with an exact solution, very precise dynamical parallaxes are obtained. For that reason, we have taken them into account in our investigation.

3. At least a couple of orbital parallaxes might have been miscalculated, that of HD 13974, and to a lesser extent, HD 76943. Since their orbits are assigned grade 1 in the ORB6, the large residuals could be due to an erroneous determination of their radial velocities. In addition, there are a few other values that could have been poorly calculated. Further studies are needed in order to clarify these discrepancies.

4. As part of our research, we obtained independent estimations of the masses of the primary and the secondary components. The individual masses were derived by comparing the CMD (absolute mag versus colour diagram) with the stellar evolution tracks

reported by Pietrinferni. The obtained values are in quite good agreement with those calculated by means of orbital, dynamical, and *Gaia* parallaxes. This has one simple logical outcome. The stellar models adopted in this work are reliable and can be used to infer further information, such as the individual age of each component in a binary system. In particular, the best agreement of the masses obtained through evolutionary tracks is found when they are compared to the masses derived using the method of dynamical parallaxes.

5. Our results show a reasonable fair correlation between the ages of the primary and secondary components of the binary systems of our sample, a best fit slope of 0.95 ± 0.05 is found. It should be noticed, however, that the obtained results could be improved by using more homogeneous and precise photometric magnitudes and colours.

ACKNOWLEDGEMENTS

The authors have made use of the WDS Catalog (https://www.usno.navy.mil/USNO/astrometry/optical - IR - prod/wds/WDS), the ORB6 (https://www.usno.navy.mil/USNO/astrometry/optical - IR - prod/wds/orb6), and the INT4 (https://www.usno.navy.mil/USNO/astrometry/optical - IR - prod/wds/int4) maintained at U.S. Naval Observatory (USNO), Washington DC. This research has made use of the SIMBAD database, operated at CDS, Strasbourg, France (The SIMBAD astronomical database, Wenger et al. 2000, http://simbad.u-strasbg.fr/simbad/) and the VizieR Service for Astronomical Catalogues (http://vizier.u-strasbg.fr/viz-bin/VizieR) operated by the Centre de donned by the Centre de données Astronomiques de Strasbourg (France).

This paper was supported by the Spanish 'Ministerio de Economía, Industria y Competitividad' under the Project AYA-2016-80938-P (AEI/FEDER, UE).

The authors thank the referee, Brian Mason, for his many valuable comments on the original manuscript, which helped to improve the article.

This research is part of Luca Piccotti's Doctoral Dissertation, proposed and directed by Prof. J. A. Docobo.

REFERENCES

Andrade M., 2019, A&A, 630, A96
Baize P., Romani L., 1946, Ann. Astrophys., 9, 13
Balega I., Bonneau D., Foy R., 1984, A&AS, 57, 31
Baraffe I., Chabrier G., Allard F., Hauschildt P. H., 1998, A&A, 337, 403
Baraffe I., Homeier D., Allard F., Chabrier G., 2015, A&A, 557, 42
Barlow D. J., Fekel F. C., Scarfe C. D., 1993, PASP, 105, 476
Barry R. K., Demory B. O., Segransan D. S., 2012, ApJ, 760, 55
Batten A. H., Fletcher J. M., MacCarthy D. G., 1989, Publ. Domin. Astrophys. Obs. Vict., 17, 1
Boden A. F., Torres G., Latham D. W., 2006, ApJ, 644, 1193
Bressan A., Marigo P., Girardi L., Salasnich B., Dal Cero C., Rubele S., Nanni A., 2012, MNRAS, 427, 127
Casagrande L., Schönrich R., Asplund M., Cassisi S., Ramírez I., Meléndez J., Bensby T., Feltzing S., 2011, A&A, 530, A138
Catanzaro G., Leto P., 2004, A&A, 416, 661
Claret A., 2007, A&A, 467, 1389
Claret A., Gimenez A., 1992, A&AS, 96, 255
Docobo J. A., Andrade M., 2013, MNRAS, 428, 321
Docobo J. A., Andrade M., 2015, AJ, 149, 45
Docobo J. A., Campo P., Horch E. P., 2017, IAU Circ., 192, 1
Docobo J. A., Campo P. P., Gomez J., Horch, Elliott P., 2018, AJ, 156, 185
Docobo J. A., Griffin R. F., Tamazian V. S., Horch E. P., Campo P. P., 2014, MNRAS, 444, 3641
Duquennoy A., Mayor M., 1991, A&A, 248, 485
Edwards T. W., 1976, AJ, 81, 245
Fekel F. C., Henry G. W., Tomkin J., 2017, AJ, 154, 120
Gaia Collaboration et al., 2016, A&A, 595A, 1
Gaia Collaboration et al., 2018, A&A, 616A, 1
Girardi L., Bressan A., Bertelli G., Chiosi C., 2000, A&AS, 141, 371
Gray D. F., 2005, The Observation and Analysis of Stellar Photospheres. Cambridge University Press, Cambridge
Hartkopf W. I., Mason B. D., 2010, IAU Circ., 170, 1
Hartkopf W. I., Mason B. D., Worley C. E., 2001a, AJ, 122, 3472
Hartkopf W. I., McAlister H. A., Mason B. D., 2001b, AJ, 122, 3480
Hummel C. A., Armstrong J. T., Buscher D. F., Mozurkewich D., Quirrenbach A., Vivekanand M., 1995, AJ, 110, 376
Hummel C. A., Armstrong J. T., Quirrenbach A., Buscher D. F., Mozurkewich D., Simon R. S., Johnston K. J., 1993, AJ, 106, 2486
Jancart S., Jorissen A., Babusiaux C., Pourbaix D., 2005, A&A, 442, 365
Malkov et al., 2018, Open Astron., 27, 62
Mason B. D., Hartkopf W. I., 2005, IAU Circ., 156, 1
Massarotti A., Latham D. W., Stefanik R. P., Fogel J., 2008, AJ, 135, 209
McAlister H. A., 1976, PASP, 88, 957
McAlister H. A., 1977, ApJ, 212, 459
McAlister H. A., 1978, ApJ, 223, 526
Palla P., Stahler S. W., 1999, ApJ, 525, 772
Parenago P. P., 1940, Astron. Zh., 17, 3
Pearce J. A., 1936, PASP, 48, 214
Pietrinferni A., Cassisi S., Salaris M., Castelli F., 2004, ApJ, 612, 168
Pourbaix D., 1998, A&AS, 131, 377
Pourbaix D., 2000, A&AS, 145, 215
Pourbaix D. et al., 2004, A&A, 424, 727
Reimers D., 1975, Mem. Soc. R. Sci. Liege, 8, 369
Scarfe C. D., Barlow D. J., Fekel F. C., 2000, AJ, 119, 2415
Sharov A. S., 1964, Soviet Ast., 7, 689
Siess L., Dufour E., Forestini M., 2000, A&A, 358, 593
Thompson W. R., 1935, Ann. Math. Statist., 6, 214
Tokovinin A. A., 1993, Ast. Lett., 19, 73
Tokovinin A. A., 2016, AJ, 152, 11
Torres G., 2004, in Hilditch R. W., Hensberge H., Pavlovski K., eds, Proceedings of the Workshop held 20-24 October 2003 in Dubrovnik, Croatia. ASP Conference Series, Vol. 318, Astronomical Society of the Pacific, San Francisco, p. 123
Torres G., Andersen J., Gimenez A., 2010, A&AR, 18, 67
VandenBerg D. A., Bergbusch P. A., Dowler P. D., 2006, ApJS, 162, 375
van Leeuwen F., 2007, A&A, 474, 653
Wenger M. et al., 2000, A&AS, 143, 9

SUPPORTING INFORMATION

Supplementary data are available at *MNRAS* online.

Table 1. ORB6 and SB9 common orbital elements.
Table 2. Calculated quantities.
Table 3. Parallaxes.
Table 5. Individual masses of the two components.
Table 7. Spectral types, temperatures, colour indices, and bolometric corrections.
Table 11. Estimation of masses and other physical quantities for the primaries.
Table 12. Estimation of masses and other physical quantities for the secondaries.

Please note: Oxford University Press is not responsible for the content or functionality of any supporting materials supplied by the authors. Any queries (other than missing material) should be directed to the corresponding author for the article.

This paper has been typeset from a TEX/LATEX file prepared by the author.